AAS 23-132

GOAL-ORIENTED GUIDANCE STRATEGY FOR BINARY ASTEROID EXPLORATION: INVESTIGATION OF DIFFERENT METRICS

Antonio Rizza[*], Carmine Giordano[†], and Francesco Topputo[‡]

Operations in proximity of minor bodies demands high levels of autonomy to achieve cost-effective safe and reliable solutions. Autonomous path and operations planning capability plays a pivotal role in this. The Deep-space Astrodynamics Research and Technology (DART) Group at Politecnico di Milano is responsible for the Mission Analysis (MA), Image Processing (IP) and Guidance Navigation and Control (GNC) subsystem design of Milani, one of the two Hera CubeSats that will be released in proximity of the Didymos binary asteroid system. A goal-oriented guidance strategy for on-board implementation is presented in this paper to achieve high level mission objectives with impulsive control capability. The methodology is based on abstract reachability analysis performed on the control domain combining model predictive control theory with artificial potential fields algorithms. The formulation of the optimization problem in a general and flexible way allows to target different goals while being compliant with an arbitrary number of mission constraints. The methodology is applied to the Milani mission scenario targeting a global coverage of the main attractor, Didymos, and detailed observations of specific features on the secondary asteroid, Dimorphos. Different metrics are investigated to achieve mission objectives leading to four application scenarios that are discussed in this work. Results are compared in terms of computational cost, convergence properties and efficiency. These results represents a step forward in enabling autonomous guidance capability for Cubesats proximity proximity operations.

INTRODUCTION

The recent growing interest in small solar system bodies such as asteroids and comets for scientific understanding, exploitation of resources and planetary defense reasons is pushing a lot the development of new technologies to better investigate these celestial bodies. Ground-based observations allow preliminary characterizations of small bodies in terms of bulk properties such as orbit, mass, shape, rotational state and surface composition. The acquisition of Range-Doppler radar data in addition to Optical and Spectroscopic observation revolutionized the way we look at asteroids allowing for precise shape and rotational state reconstruction.[1] A drastic improvement in the body characterization can be obtained with in-situ observations with the use of specialized and instrumented probes. Historically the easiest way of performing proximity observations is achieved designing a spacecraft trajectory that intersects the target on its way towards its final destination

[*]PhD Candidate, Department of Aerospace Science and Technology, antonio.rizza@polimi.it
[†]Postodctoral Research Fellow, Department of Aerospace Science and Technology, carmine.giordano@polimi.it
[‡]Full Professor, Department of Aerospace Science and Technology, francesco.topputo@polimi.it

performing a far flyby. This strategy usually provide, however, low resolution images with very limited observation windows. Rendezvousing with a Small Body and hovering in its proximity is a challenging engineering task because it requires precise trajectory control and accurate navigation in a low gravity highly perturbed dynamical environment. Many robotic missions successfully performed scientific operations in proximity of asteroids, comets and minor planets. Fundamental milestones have been marked in the last two decades by missions such as NEAR,[2] Dawn,[3] OSIRIS-REx,[4] Hayabusa,[5] Hayabusa 2,[6] and Rosetta,[7] throwing the bases of modern deep-space exploration techniques. Recent resonance to the field is doubtless provided by DART:[8] the kinetic impactor developed within the framework of the Asteroid Impact Deflection Assessment (AIDA) program, an ESA-NASA collaboration to test the deflection capability of a kinetic impactor on potentially hazardous Near Earth Objects (NEO). DART targeted and successfully impacted in September 2022 the secondary asteroid of the Didymos-Dimorphos binary system. It is the first time in history that such kind of complex dynamical systems are observed in close proximity, and the data collected by the probe will be subject of study for years. The ConOps of past missions have many common aspects, a preliminary characterization of the targets is generally performed from a safe distance, following orbits or hyperbolic arcs accurately designed on Earth. Knowledge of the system and its dynamical environment are initially provided only via ground observations. The initial proximity phase helps refining this preliminary knowledge paving the way to closer approaches. This tasks have always been performed by large instrumented probes with heavily margined trajectory control capability and limited autonomy on-board. Nowadays the Space exploration field is withstanding a transition towards the use of CubeSats, and miniaturized platforms in general, for the systematic exploration of the Solar System.[9] Their use aims at performing riskier tasks and operate in multi-agent scenarios while cooping with limited resources. This trend is demanding always higher levels of autonomy on-board to achieve cost-effective safe and reliable solutions, particularly for what concern proximity guidance and navigation. Classical trajectory optimization typically implies the solution of an optimal control problem to get a reference trajectory to be followed by the spacecraft. This optimization generally requires the minimization of fuel, time-of-flight or a combination of them to move from a given initial state to a given final state in the configuration space. This approach works well when an interplanetary transfer is designed but exhibits some drawbacks when facing the challenges of small bodies proximity operations. Small body environment is characterized by high uncertainty affecting the dynamics governing the spacecraft motion and strong perturbation due to the predominant effect of solar radiation pressure. Moreover, the body shape is generally only partially known and it may be difficult to identify a priori the path to achieve the best characterization of the target since this requires a mapping between given geometrical configurations and observation requirements. These effects leads to high dispersion and uncertainties which make the design of the proximity control a challenging task. An innovative concept developed in recent years is proposing a paradigm shift towards autonomous goal-oriented approaches. The idea is that the probe is provided with the high-level objectives of the mission and the trajectory is computed autonomously on-board within a continuous replanning framework to best achieve the assigned tasks. Of paramount importance in this field is, to the authors' opinion, the work by D. Surovik,[10] where he proposes a reachability analysis exploration scheme performed in the control domain to compute optimal impulsive manoeuvrers to maximize the observation of surface feature within a receding horizon model predictive control framework. The same concept is extended by Capolupo[11] to the case of global mapping. A similar methodology is also exploited in Earth's orbit for the development of Simultaneous Localization And Mapping (SLAM) techniques in proximity of artificial objects.[12]

This work presents an innovative goal-oriented guidance methodology with a formulation that is flexible and adaptable to different mission scenarios. The structure of this paper is the following: first the problem formulation is presented, together with a general framework to produce global and feature-based observation models. Then the numerical technique to solve the optimization problem, based on abstract reachability analysis is illustrated. Finally, four application scenarios are shown and results of the approach are discussed.

PROBLEM STATEMENT

The idea behind the proposed methodology is based on the work on abstract reachability analysis performed by Surovik[10] and Capolupo.[11] The idea is to target mission objectives in an abstract space and periodically replanning the spacecraft trajectory to take into account accomplished tasks, dispersion, knowledge uncertainty and updates in the target's characterization. Before presenting the methodology it is necessary to give some definitions. Referring to Figure 1 the spacecraft state at the a given epoch t_0 after the impulsive manoeuvre $\mathbf{u}_0 \in U_0$ is given by $\mathbf{x}_0^+ = \mathbf{x}_0^- + \mathbf{u}_0$, with $\mathbf{x}_0^-$ being the pre-manoeuvring state. The resulting trajectory flow, $\mathbf{x}(\mathbf{u}_0, t_0; t)$ is mapped into a measurements vector $\mathbf{y}_i(\mathbf{x}) \in Y_i \subset \mathbb{R}^{N_m}$, where Y_i are a set of measurement spaces associated either with a specific feature on the body surface or with some global observation property, and N_m the number of considered measurements. Mission objectives defines in the Y_i spaces bounded

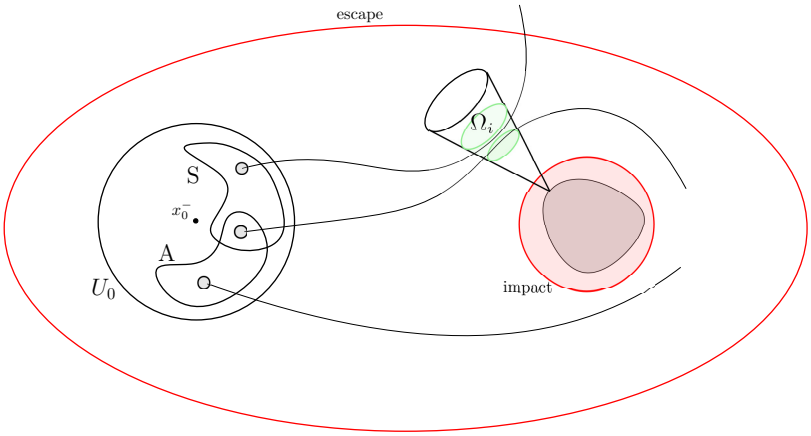

Figure 1: Graphical illustration of the important sets.

observation regions indicated with $\Omega_i \subset Y_i$, mapping for example required surface resolution and illumination conditions with range and phase-angle constraints. This allows to define the Science region S as the portion of the control domain U_0 that leads to a crossing of the observation regions, i.e.:

$$S := \{\mathbf{u}_0 \in U_0 : \exists t \in [t_0, t_h], \exists i \in [1, N_f] : \mathbf{y}_i(\mathbf{u}_0, t) \in \Omega_i\} \tag{1}$$

In Eq.(1) t_h and N_f are respectively the horizon epoch and the number of features to be observed. The former one indicates the latest epoch in which the next manoeuvrer is to be performed, while the actual manoeuvring epoch is referred to as t_m. Limiting the search of the optimal solution only to the S region would however not consider the fact that there may be operational constraints and forbidden regions in the configuration space. These regions would take into account for impacts, escapes, flight to the night side and any other constraint on the feasible spacecraft path. This constraints can be expressed in general through the inequality constraint $\mathbf{g}(\mathbf{x}, t) \leq 0$ leading to the

definition of an Admissible region A:

$$A := \{\mathbf{u}_0 \in U_0 : \mathbf{g}(\mathbf{x}(\mathbf{u}_0, t), t) \leq 0, \forall t \in [t_0, t_h]\} \tag{2}$$

For the cases discussed in this work the admissible region is given by the satisfaction of the following constraints:

- minimum distance from Didymos larger than 500 m (to avoid impact on Didymos);
- minimum distance from Dimorphos larger than 180 m (to avoid impact on Dimorphos);
- maximum distance from the system centre of mass lower than 50 km (to avoid escape from the system);
- spacecraft phase angle lower than 130 deg (to remain in the day side).

The last constraint stems from navigation requirements. Milani relies on vision-based optical navigation techniques to reconstruct its state on-board.[13] In order to reduce dispersion and manoeuvring uncertainties, firing should be performed when a good knowledge of the state is available. This may not be possible when the spacecraft is flying in the nigh-side. As will be shown later on in this paper, this constraint often leads to an hyperbolic hovering approach to the asteroids, which is indeed the current baseline for the mission.[14] The last important domain to be defined is the dual of A for the manoeuvring time. Defining a set of constraints on t_m, namely $\mathbf{h}(t_m) \leq 0$ a region T can be defined as in Eq. 3.

$$T := \{t_m \in [t_0, t_h] : \mathbf{h}(t_m) \leq 0\} \tag{3}$$

In this work, unless differently specified, it is only imposed $t_m - t_0 \geq 1$ day. This type of constraint stems from the need of having manoeuvrers sufficiently distributed in time to allow convergence of the navigation solution before the successive planning cycle. The optimization problem is then given by the minimization of a cost function J over the impulsive initial control and the successive manoeuvring time t_m as reported in Eq. 4.

$$\begin{cases} \min\limits_{\mathbf{u}_0, t_m} J(\mathbf{u}_0, t_m) \text{ s.t.} \\ \qquad \mathbf{u}_0 \in A \cap S \\ \qquad\quad t_m \in T \end{cases} \tag{4}$$

The objective function proposed in this methodology is a general purpose cost function linked with the time spent inside observation regions given by Eq. 5.

$$J(\mathbf{u}_0, t_m) = -\frac{1}{N_f} \sum_{i=1}^{N_f} min\left(1, \frac{1}{\Delta t_i} \int_{t_0}^{t_m} \omega_i(\mathbf{y}_i(\mathbf{u}_0, \tau), \tau) d\tau + g_{0i}\right) \tag{5}$$

Where Δt_i is the required observation time for the i-th feature, ω_i is a potential function evaluated on the measurement space Y_i and g_{0i} is the normalized integral computed at the previous planning cycle. The *min* function is needed to saturate the cost function when a feature has been fully observed. A general form of ω_i may be the one given in Eq. 6, with m_{ij} a metric indicating the distance of the j-th quantity from the observation region Ω_i.

$$\omega_i = \prod_{j=1}^{N_m} m_{ij} \tag{6}$$

If a boolean approach is adopted, and observation regions Ω_i are hypercubes in the Y_i space delimited by the lower and upper bounds y_{ij}^- and y_{ij}^+, m_{ij} can be expressed as in Eq. (7).

$$m_{ij} = \begin{cases} 1 & y_{ij}^- \leq y_{ij} \leq y_{ij}^+ \\ 0 & \text{otherwise} \end{cases} \tag{7}$$

In this case the integral term in the cost function gives exactly the time spent spent by the spacecraft inside the observation region Ω_i. At this point an observation model needs to be defined to properly map the configuration space X into the measurement space Y. Two observation models are developed and presented in this work: inertial and rotating. In the former one the asteroid is modelled with a single feature ($N_f = 1$) and two measures ($N_m = 2$) are considered: the range ρ from the asteroid centre of mass and the phase angle α. Observation regions are then defined as cone sections in the X space and rectangles in the Y space as shown in Figure 2. In the rotating model, instead,

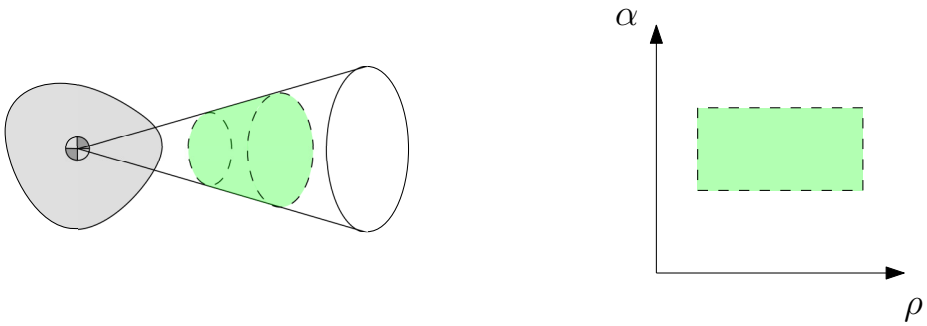

Figure 2: Inertial observation regions. On the left the observation region in the X space while on the right its mapping in the Y space.

an arbitrary number of features is defined ($N_f > 1$) and three measures ($N_m = 3$) are considered: the range ρ_i, the spacecraft declination δ_i, and the Sun declination β_i with respect to each feature. Here although observation regions assume complex, time dependent shapes in the X space, they are still mapped into cubes in each of the Y_i space, as shown in Figure 3. To the authors' opinion this is the real advantage of performing the optimization in the abstract domain.

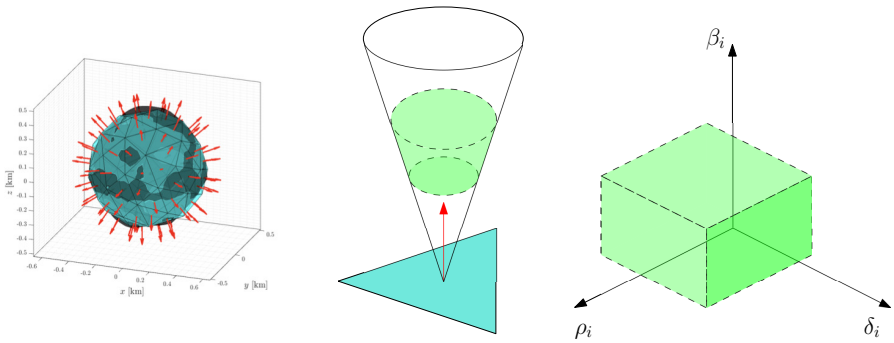

Figure 3: Rotating observation regions. On the left the surface feature, in the centre one observation regions in the X space and, on the right its mapping in its Y_i space.

METHODOLOGY

The methodology proposed in this paper to solve the optimization problem of Eq.(4) consists in performing a reachability analysis on the control domain U_0 supported by an heuristic mesh refinement. The procedure is summarized in Figure 4. The first step is to generate a uniform initial mesh $U_0^{(0)}$ on the control domain. The problem of uniformly sampling a sphere is non trivial, in this work this is achieved by generating a series of concentric Fibonacci's lattices* with different surface density. This property is set in order to have uniform volumetric density of the samples. In partic-

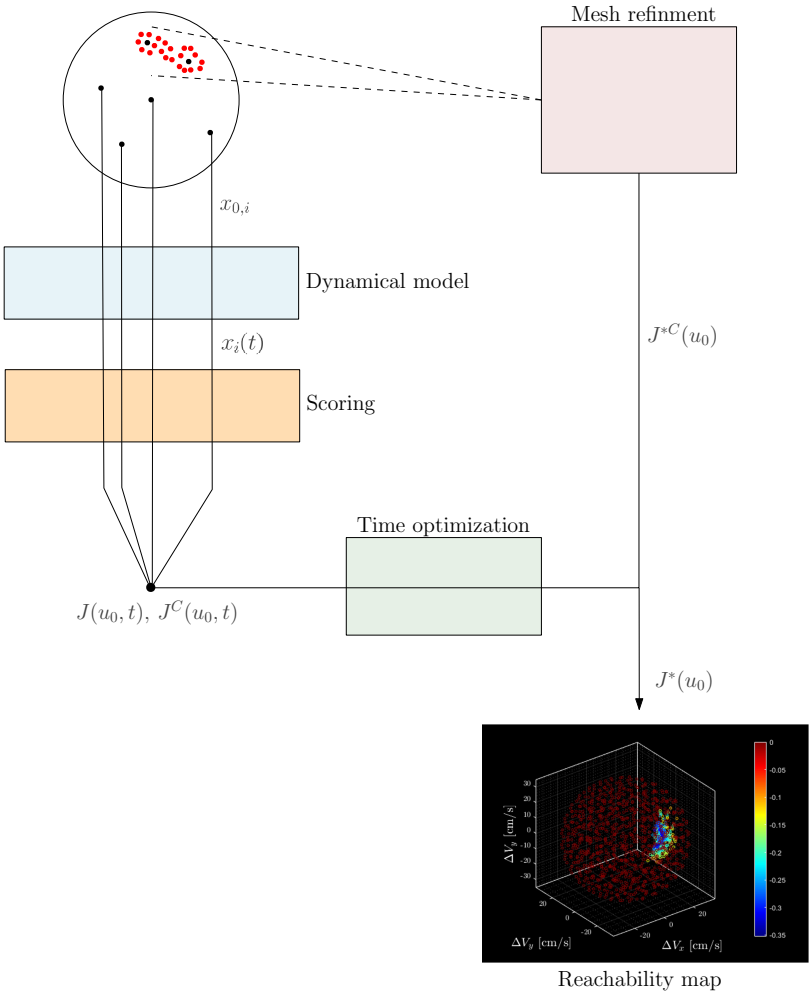

Figure 4: Numerical approach: rechability analysis and heuristic mesh refinement.

ular the pseudocode used to generate this mesh is shown in Algorithm 1. Each point $\mathbf{u}_{0,i}$ of $U_0^{(0)}$, corresponding to a different initial condition $\mathbf{x}_{0,i}^+$, is then propagated forward in time from t_0 to t_h. A non-dimensional ephemeris model is used to integrate the dynamics in proximity of the binary system; in particular the point mass gravitational effect of the two asteroids and the Sun is considered, together with the perturbation due to Solar Radiation Pressure (SRP). For the purpose of this work, the integration is performed with the MATLAB variable-step solver ode113. The propagated

*http://extremelearning.com.au/evenly-distributing-points-on-a-sphere/ last retrived on 16th Jan 2023

Algorithm 1: Generation of initial mesh $U_0^{(0)}$

$\rho_{v,mesh} \leftarrow$ Selected mesh volumetric density
$N_r \leftarrow$ Number of layers in the radial direction
$U_0^{(0)} = [\,] \leftarrow$ Initialize mesh
$r_c = [0, 0, 0] \leftarrow$ Centre of the mesh
for $k = 0 : N_r$ **do**
  $r_k = \frac{k}{N_r} \leftarrow$ Define radius of mesh layer
  $n = \lfloor \frac{4}{3}\pi r_k^3 \rho_{v,mesh} \rfloor \leftarrow$ Number of points on the fibonacci distrubution
  $[U_k] = \texttt{generate\_fibonacci\_distribution}(r_c, r_k, n)$
  $U_0^{(0)} = [U_0^{(0)}, U_k] \leftarrow$ Append new mesh layer to the mesh
end

trajectories $\mathbf{x}_i(t) = \mathbf{x}(\mathbf{u}_{0,i}, t)$ are then scored with the selected cost function. In order to take into account the constraints in Eq.(4) an augmented cost function $\tilde{J}(\mathbf{u}_{0,i}, t) = a(\mathbf{u}_{0,i})s(\mathbf{u}_{0,i})J(\mathbf{u}_{0,i}, t)$ is computed using the boolean model for ω_i reported in Eq.(7). Where $a, s = 1$ if $\mathbf{u}_{0,i}$ belongs respectively to A and S. Then, a time optimization is performed, identifying for each point of the mesh the manoeuvre time t_m that minimize the cost function, resulting in the map $J^{*(0)}(\mathbf{u}_0)$. To make the computation affordable, the mesh $U_0^{(0)}$ needs to be relatively small, in this work the control domain is restricted to a sphere with radius of 35 cm/s, to be in line with the Milani spacecraft ΔV budget,[14] and an initial mesh with 300 points is considered. This discretization is clearly too rough to properly characterize the reachability map, therefore a mesh refinement is needed. In literature this problem is typically faced using an heuristic approach,[10,11] exploiting the structure of the map to identify regions of high interested to be refined. A similar strategy is adopted in this work and presented in the following. First of all the boolean information embedded in $\tilde{J}(\mathbf{u}_{0,i}, t)$ is not enough to assess properly which unexplored areas of the control domain may contain high score trajectories, moreover, if the initial sampling is significantly limited or if the targeted observation regions are very small, the initial mesh may not contain any intersection between the admissible and the science region. In this case the propagation of $U_0^{(0)}$ may simply lead to a null field. To avoid this issue a relaxation of the potential ω_i is performed defining a continuous metrics m_{ij}^C as in Eq.(8). With $\bar{y}_{ij}$ being the geometric centre coordinates of the observation region Ω_i.

$$m_{ij}^C = e^{-|y_{ij} - \bar{y}_{ij}|} \tag{8}$$

With the use of this potential a continuous cost function $J^C(\mathbf{u}_{0,i}, t)$ is computed together with its augmented counterpart $\tilde{J}^C(\mathbf{u}_{0,i}, t) = a(\mathbf{u}_{0,i})J^C(\mathbf{u}_{0,i}, t)$. This time only the admissible constraint is considered because non-zero values are desired even outside of science regions. The time optimized map obtained in this case will be denoted as $J^{*C(0)}(\mathbf{u}_0)$. The mesh refinement scheme implemented in this work consists in identifying the n_{best} nodes in the mesh with the lowest cost function and refine their neighbourhood . The pseudocode of the algorithm is reported in Algorithm 2. The mesh refinement procedure is repeated a few times, recomputing at each cycle the map $J^{*(k)}$ on the new mesh. If the refinement algorithm is called and none of the new nodes has reached a better score than the previous iteration, e.i. $U_{0,reduced}^{(k)} = \emptyset$, the algorithm is stopped. For the results reported in this work it is selected $n_{best} = 10$, $n_{max,iteration} = 5$. Once the mesh refinement procedure is over the result is a non uniform map $J^*(\mathbf{u}_0)$ from which the optimal solution $\mathbf{u}_0^*$ and its associated manoeuvring time t_m^* are extracted. This planning cycle is repeated until mission objectives are

Algorithm 2: Heuristic mesh refinement

$n \leftarrow$ Number of points in the refined sub-meshes
$n_{best} \leftarrow$ Maximum number of refinement nodes
$U_0^{(k)} \leftarrow$ k-th iteration of the mesh
$J^{*(k)} \leftarrow$ k-th iteration of the continuous reachability map
$i_s \leftarrow$ index of nodes whose neighbourhood has already been refined
$[U_{0,reduced}^{(k)}, J_{reduced}^{*(k)}] = \texttt{reduce\_mesh}(U_0^{(k)}, i_s) \leftarrow$ compute subsets to be refined
$[U_{0,best}^{(k)}, J_{best}^{*(k)}] = \texttt{identify\_best\_solutions}(U_0^{(k)}, J^{*(k)}, n_{best}) \leftarrow$ identify n_{best} solutions
$U_0^{(k+1)} = [U_0^{(k)}] \leftarrow$ Initialize new mesh
for $l = 1 : \texttt{size}(U_{0,best}^{(k)})$ **do**
  $u_0^{(l)} = U_{0,best}^{(k)}(l) \leftarrow$ Centre of the new refined mesh
  $[r_l] = \texttt{closest\_node\_range}(u_0^{(l)}, U_{0,best}^{(k)}) \leftarrow$ Range to the closest node in the mesh
  $[U_l] = \texttt{generate\_fibonacci\_distribution}(u_0^{(l)}, r_l, n)$
  $U_0^{(k+1)} = [U_0^{(k+1)}, U_l] \leftarrow$ Append new mesh layer to the mesh
end

accomplished or a maximum number of planning cycles is performed. The first condition is verified when $g = 1$, where g is the normalized overall time spent within the observation regions, as shown in Eq.(9).

$$g(t) = \sum_{i=1}^{N_f} min\left(\frac{1}{\Delta t_i}\int_{t_0}^{t}\prod_{j=1}^{N_m} m_{ij}d\tau + g(t_0), 1\right) \tag{9}$$

One final remark regarding the methodology is necessary. The discussed objective function does not weight the magnitude of the control action. This effect is already embedded in the fact that the reachability analysis is restricted to a limited control domain, however one may want to take this into account during the optimization. In this case the augmented cost function J_{full} reported in Eq. (10) can be used.

$$J_{full}(\mathbf{u}_0) = (1 - \alpha_u(g_{0i}))J^*(\mathbf{u}_0) + \alpha_u(g_{0i})a(\mathbf{u}_0)s(\mathbf{u}_0)\frac{||\mathbf{u}_0|| - min||\mathbf{u}_0||\Big|_{A\cap S}}{max||\mathbf{u}_0||\Big|_{A\cap S}} \tag{10}$$

This formulation is used in this work, with the weighting coefficient $\alpha_u = \frac{1}{2}(1-\frac{1}{N_f}\sum_{i=1}^{N_f} g_{0i})$. This additional potential in the objective function is beneficial for two reasons: it avoids having plateau in the reachability map and, thanks to the dependence of α_u from the mission status, facilitates the algorithm convergence when the goals achievement is close to one.

TEST CASES AND RESULTS

The Deep-space Astrodynamics Research and Technology (DART) Group at Politecnico di Milano is responsible for the Mission Analysis,[14] Image Processing,[15] and GNC[13] subsystem design of Milani, one of the two CubeSats carried on-board Hera,[16] the european contribution to the AIDA

program. Hera and its two CubSats will rendesvous with the Didymos binary system in early 2027 to characterize the post impact environment.[17] Didymos is a binary Near-Earth Asteroid (NEA) of S-type discovered in 1996 formed by Didymos, or D1 (the primary) and Dimorphos, or D2 (the secondary). The analysis in this paper are made with the pre-impact orbital properties of the system summarized here. The two asteroids share the same equatorial plane on which their relative motion occurs, D2 is tidally locked with with D1 with a rotation period of the primary $T_{D1} = 2.26$h and a rotation and revolution period of the secondary $T_{D2} = 11.92$ h.[14] In this section Milani is used as a test case to validate this approach in the proximity of the binary systems. Four applications are shown: first the case of global mapping of D1 using an inertial observation model is discussed underlining strength and limitations of this approach, then the same goal is targeted using a rotating observation model. Monte Carlo (MC) simulations are performed to assess the robustness and success rate for the two approaches. In both cases mission performances are assessed using the rotating observation model being the one that best represents the effective coverage of the target. The third application presented here is again on the global coverage of D1 but imposing this time the additional operative constraints of a given manoeuvring schedule. Finally, the last application is on the observation of the post-impact crater on D2. An inertial frame centred in the system barycentre and aligned with the ECLIPJ2000 frame is used for propagation and inertial observation regions definition while body fixed rotated frames are used for the rotating approach.

Global mapping of D1 - Rotating approach

In the rotating approach, the main asteroid shape model is discretized to obtain an observation model with 96 features, intended as regions on the surface to be observed, as shown in Figure 3. For each of them the targeted observation region is defined by a range from the feature 8.640 km $\leq \rho \leq 10.940$ km, a spacecraft declination over the surface 60 deg $\leq \delta_i \leq 90$ deg, and a Sun declination over the surface dependent from the feature latitude LAT_i. In particular: 70 deg $\leq \beta_i \leq 90$ deg if 0 deg $\leq LAT_i \leq 10$ deg, 45 deg $\leq \beta_i \leq 90$ deg if 10 deg $< LAT_i \leq 30$ deg, 0 deg $\leq \beta_i \leq 90$ deg if 30 deg $< LAT_i \leq 90$ deg. This differential observation constraints are selected to grant the satisfaction of scientific requirements in the equatorial region[14] while granting the feasibility of valid observations at higher latitudes. The required observation time for each feature is set to 1 hour. A MC analysis is performed on 500 random samples of $\mathbf{x}_0^-$ to assess the success rate and the time required to achieve global coverage. Position and velocity direction are generated with a standard uniform distribution within the spacecraft operative region while, a normal probability distribution with mean of 3 cm/s and standard deviation of 3.3 mm/s is selected for the velocity magnitude. Results of the simulations are reported in Figure 5. It can be seen that operative constraints (impact, escape, permanence in the day side) are never violated and the planned trajectories are hyperbolic hovering arcs. Moreover all the trajectory reach global coverage of D1 in less than 20 days. Even if the approach successfully target all 96 observation regions, it is however computationally demanding because of the large number of $\mathbf{y}_i$ vectors that needs to be computed. An alternative strategy is presented in the following section.

Global mapping of D1 - Inertial approach

With the inertial approach, only one feature located in D1 centre of mass is considered. The reachability map is computed targeting the following observation region: 8.640 km $\leq \rho \leq 10.940$ km and 0 deg $\leq \alpha \leq 70$ deg with a required observation time of 3 days. Since metric comparison is intended, the goal in Eq. (9) is still computed using all the 96 features of the previous case. A second MC analysis is performed using the same initial conditions of the rotating case and results

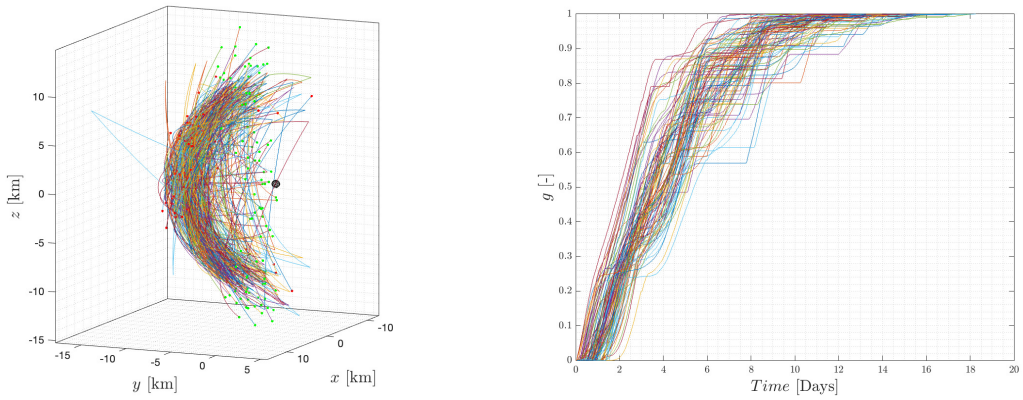

Figure 5: Rotating approach. On the left the trajectory envelope in the inertial frame ECLIPJ2000, on the right the goal achieved by the mission as a function of time.

are shown in Figure 6. All the trajectories still comply with operative constraints and the resulting arcs between manoeuvres are still hyperbolic trajectories. However, the goal achievement exhibits an asymptotic behaviour. This was of course an expected trend because here the optimization is not informed on the features' location but, the interesting thing, is that still a significant percentage of trajectories gets to very high scores. In particular, looking at Figure 7 it can be seen that more than

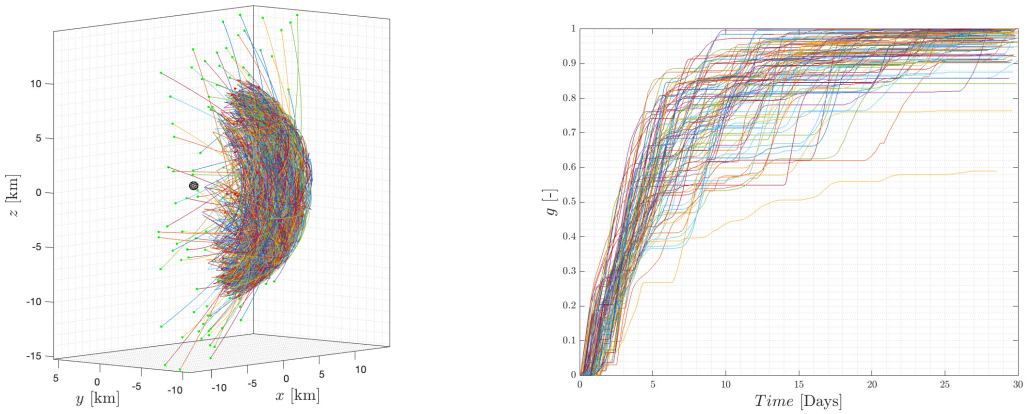

Figure 6: Inertial approach. On the left the trajectory envelope in the inertial frame ECLIPJ2000, on the right the goal achieved by the mission as a function of time.

90% of the initial samples, leads to an effective global coverage of D1 higher than 90% even if more time, and thus fuel, is needed. This is a surprising results considering the relatively low computation effort of this approach. The few trajectories that stall at early mission stage are the ones that keep hovering over the same hemisphere limiting the observation of the features on the other.

Compliance with working week

The third study case presented here is the one in which the approach feasibility to the potential need of having a manoeuvring schedule synchronized with ground operations is assessed. To do

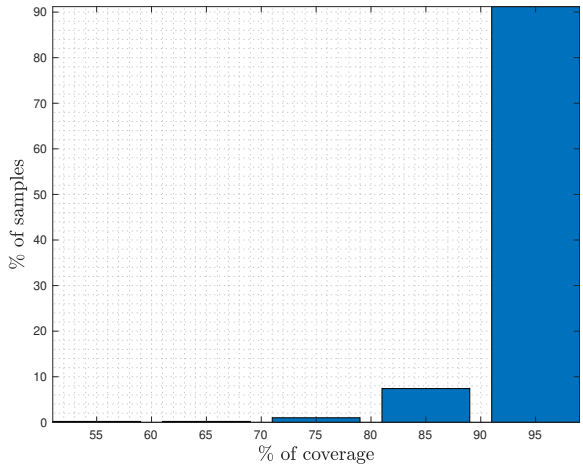

Figure 7: Histogram showing the success rate of the randomly sampled MC distribution for the inertial approach.

this, the region T of Eq. (3) is defined by imposing a fixed t_m and following a 3-4 days pattern from one arc to the next one in order to be aligned with the working week on-ground. This is also the same pattern followed by the Milani spacecraft during its Far Range Phase (FRP) aimed at giving a global characterization of the asteroid.[14] The reachability map is computed by targeting all the surface features, like for the rotating case, but this time only one trajectory is considered. The initial time t_0 for the computation is set a few seconds before the FRP injection manoeuvre of Milani and, the initial state $\mathbf{x}_0^-$ is taken from the ephemeris of the spacecraft. The idea is to compare performances for the two cases in terms of coverage and ΔV. Trajectory comparison and goal achievement are shown in Figure 8. It is observed that the trajectory produced by the planner leads to global coverage of D1 according to the imposed requirements while Milani trajectory leads to a lower score. This is due to the fact that the trajectory computed by the algorithm covers higher

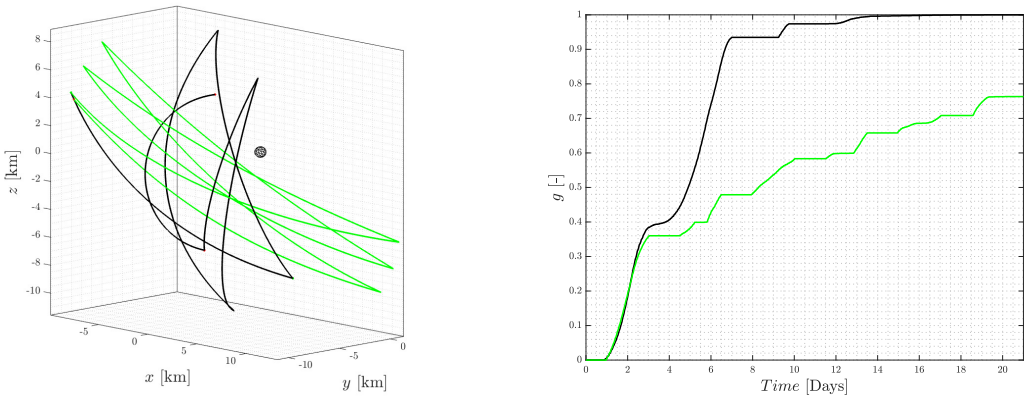

Figure 8: Compliance with working week. On the left trajectory comparison in the inertial frame ECLIPJ2000, on the right the goal achieved by the mission as a function of time. In black the outcome of the planner, in green the Milani one.

latitudes, thus allowing detailed observations of the polar regions differently. This is clearly seen in Figure 9 where both trajectories are plotted in D1 rotating body frame and the achieved coverage of each feature is shown in the case of Milani. Also from a ΔV point of view this approach results

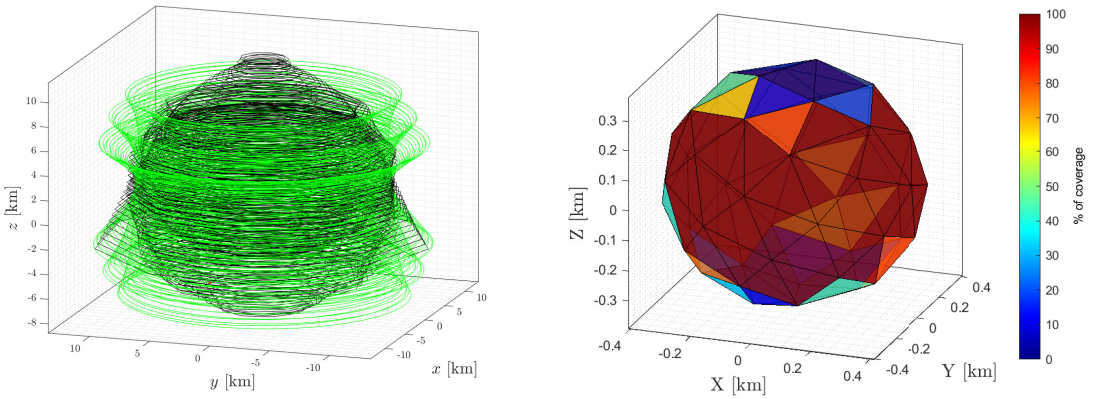

Figure 9: Performance comparison. On the left the produced trajectory is compared with Milani's one in the rotating asteroid frame of D1. On the right the coverage map on D1 is shown for Milani trajectory, showing limited observation of the polar regions.

more convenient leading to a deterministic budget of 91.94 cm/s against the 115.56 cm/s of the nominal mission profile during the same phase [†]. Note that, the mission analysis of Milani is not designed to achieve a global coverage of D1 and it takes into account lots of other constraints such as the ones deriving from communication requirements and observations of D2. Moreover, differently from the Milani study, neither a knowledge or dispersion analysis are performed at this stage on the proposed methodology to assess the robustness of the approach against navigation and firing uncertainty. Therefore, this is not meant to be a proof of the goodness of one trajectory with respect to the other but simply a performance comparison against a known trajectory.

Observation of the crater on D2

The last test case presented in this work is the observation of a specific feature on the secondary asteroid: DART impact crater. To achieve this, a mixed approach is used among the ones illustrated so far planning each arc in a twofold pipeline. First a targeting of the observation region associated with the crater is attempted, if this fails because the feature is not observable with those initial conditions, the optimization switches to an inertial approach, leading to a repositioning in front of D1. This basically works as a re-phasing manoeuvre between the spacecraft and D2. To set up the simulation, the rotating observation region is defined by 1.96 km $\leq \rho \leq 2.78$ km, 45 deg $\leq \delta \leq 90$ deg and, 75 deg $\leq \beta \leq 90$ deg, while the inertial observation region is given by 1 km $\leq \rho \leq 5$ km, 0 deg $\leq \alpha \leq 10$ deg. The resulting trajectory is shown in Figure 10 while the goal achievement is reported in Figure 11. Interestingly, the initial part of the trajectory follows an hyperbolic arc hovering approach, during which the goal gradually increases. However, after a few cycles, a feasible set of closed trajectories with high phase angle is found to be the optimal solution. Differently from the hovering approach with open trajectories, see for example Figure 8, the closed orbits leads to a linear behaviour of the goal achieved also when approaching the mission success.

[†]Values retrieved from internal documents on the Milani mission analysis.

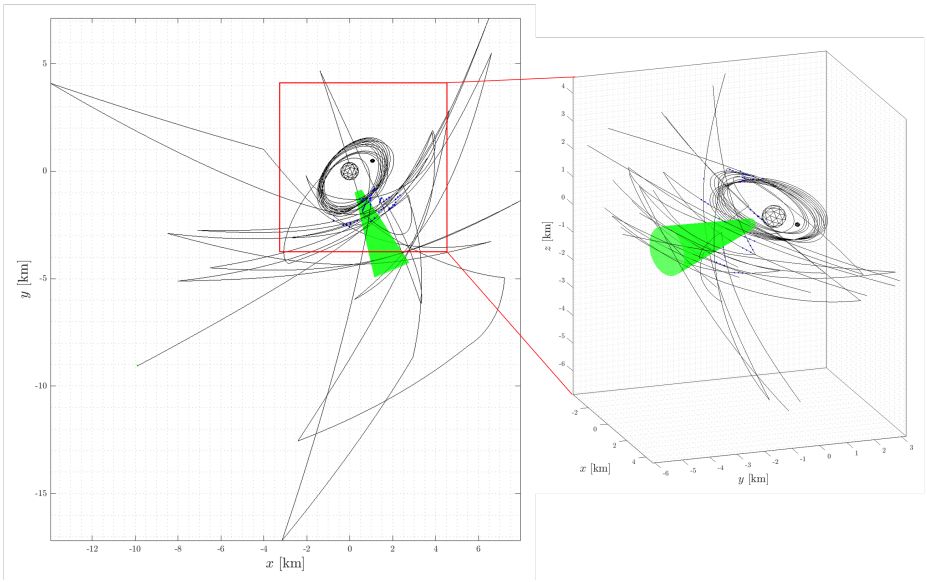

Figure 10: Crater observation (to be updated)

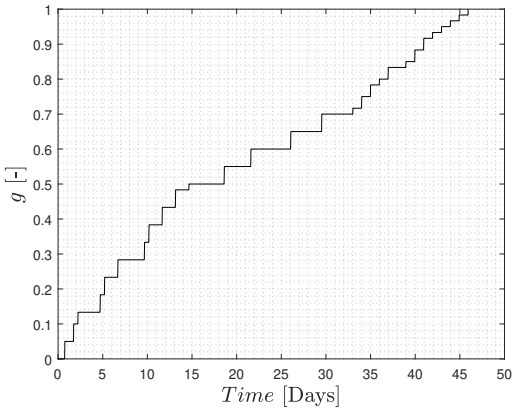

Figure 11: Goal achieved by the mission as a function of time.

Clearly the feasibility of such orbit would need to be assessed at least by performing dispersion analysis which from previous studies on Milani resulted to significantly impact the mission close approach. However this is out of the scope of this paper which is only to present some preliminary open loop results with the presented methodology.

CONCLUSIONS AND FUTURE WORK

In this paper, a general purpose formulation is provided for the problem of performing goal-oriented proximity operations to small bodies. To the authors' knowledge this is the first time that this kind of approach is systematically applied to a binary asteroid system considering a realistic set of operational constraints and observation requirements on both attractors. Four application scenarios are discussed for both global mapping and features observation. Preliminary results are shown considering only open loop trajectories with no navigation or dispersion uncertainty. However, these

results are very promising: the rotating approach allows to always achieve global coverage of the target, the inertial approach is computationally cheaper but provides still pretty good results even on its own. Combining the two a close proximity guidance strategy is presented capable of performing detailed observations of surface features with complex and time dependent observation constraints. In general this work indicates that abstract reachability analysis for spacecraft proximity guidance is a field that is worth investigating further. Future work consists in performing closed-loop simulations with on-board navigation in the loop, processor-in-the-loop analysis are needed to assess the actual computation need of the algorithm in terms of CPU and RAM. The numerical methodology could be refined by substituting the heuristic mesh refinement with a more sophisticated gradient based method and, finally, it would be interesting to extend the methodology to additional metrics and objective functions such as one involving SLAM strategies whose interest is spreading a lot in recent years.

REFERENCES

[1] D. J. Scheeres, *Orbital motion in strongly perturbed environments: applications to asteroid, comet and planetary satellite orbiters*. Springer, 2016.

[2] D. W. Dunham, J. V. McAdams, and R. W. Farquhar, "NEAR mission design," *Johns Hopkins APL technical digest*, Vol. 23, No. 1, 2002, pp. 18–33.

[3] M. D. Rayman, "Lessons from the Dawn mission to Ceres and Vesta," *Acta Astronautica*, Vol. 176, 2020, pp. 233–237.

[4] O. Barnouin, M. Daly, E. Palmer, C. Johnson, R. Gaskell, M. Al Asad, E. Bierhaus, K. Craft, C. Ernst, R. Espiritu, *et al.*, "Digital terrain mapping by the OSIRIS-REx mission," *Planetary and Space Science*, Vol. 180, 2020, p. 104764.

[5] M. Yoshikawa, J. Kawaguchi, A. Fujiwara, and A. Tsuchiyama, "The Hayabusa mission," *Sample Return Missions*, pp. 123–146, Elsevier, 2021.

[6] S.-i. Watanabe, Y. Tsuda, M. Yoshikawa, S. Tanaka, T. Saiki, and S. Nakazawa, "Hayabusa2 mission overview," *Space Science Reviews*, Vol. 208, No. 1, 2017, pp. 3–16.

[7] K.-H. Glassmeier, H. Boehnhardt, D. Koschny, E. Kührt, and I. Richter, "The Rosetta mission: flying towards the origin of the solar system," *Space Science Reviews*, Vol. 128, No. 1, 2007, pp. 1–21.

[8] A. F. Cheng, A. S. Rivkin, P. Michel, J. Atchison, O. Barnouin, L. Benner, N. L. Chabot, C. Ernst, E. G. Fahnestock, M. Kueppers, *et al.*, "AIDA DART asteroid deflection test: Planetary defense and science objectives," *Planetary and Space Science*, Vol. 157, 2018, pp. 104–115.

[9] R. Walker, D. Binns, C. Bramanti, M. Casasco, P. Concari, D. Izzo, D. Feili, P. Fernandez, J. G. Fernandez, P. Hager, *et al.*, "Deep-space CubeSats: thinking inside the box," *Astronomy & Geophysics*, Vol. 59, No. 5, 2018, pp. 5–24.

[10] D. A. Surovik, *Autonomous mission design in extreme orbit environments*. PhD thesis, University of Colorado at Boulder, 2016.

[11] F. Capolupo, T. Simeon, and J.-C. Berges, "Heuristic Guidance Techniques for the Exploration of Small Celestial Bodies," *IFAC-PapersOnLine*, Vol. 50, No. 1, 2017, pp. 8279–8284.

[12] M. Maestrini, "Satellite inspection of unknown resident space objects," 2022.

[13] M. Pugliatti, A. Rizza, F. Piccolo, V. Franzese, C. Bottiglieri, C. Giordano, F. Ferrari, and F. Topputo, "The Milani mission: overview and architecture of the optical-based GNC system," *AIAA Scitech 2022 Forum*, 2022, p. 2381.

[14] C. Bottiglieri, F. Piccolo, A. Rizza, C. Giordano, M. Pugliatti, V. Franzese, F. Ferrari, F. Topputo, *et al.*, "Trajectory design and orbit determination of Hera's Milani CubeSat," *2021 AAS/AIAA Astrodynamics Specialist Conference*, 2022, pp. 1–15.

[15] M. Pugliatti, V. Franzese, A. Rizza, F. Piccolo, C. Bottiglieri, C. Giordano, F. Ferrari, F. Topputo, *et al.*, "Design of the on-board image processing of the Milani mission," *44th AAS Guidance, Navigation and Control Conference*, 2022, pp. 1–21.

[16] P. Michel, M. Küppers, and I. Carnelli, "The Hera mission: European component of the ESA-NASA AIDA mission to a binary asteroid," *42nd COSPAR Scientific Assembly*, Vol. 42, 2018, pp. B1–1.

[17] P. Michel, M. Küppers, A. C. Bagatin, B. Carry, S. Charnoz, J. De Leon, A. Fitzsimmons, P. Gordo, S. F. Green, A. Hérique, *et al.*, "The ESA Hera mission: detailed characterization of the DART impact outcome and of the binary asteroid (65803) Didymos," *The Planetary Science Journal*, Vol. 3, No. 7, 2022, p. 160.